BB

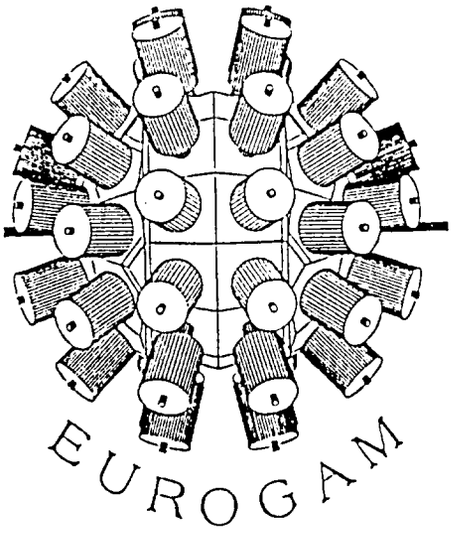

FRANCE - UK

Collaboration

Detailed Level Scheme of ^{151}Tb and the Feeding of the Normal-Deformed States by the Superdeformed Bands

C.M.Petrache[1], G.Duchêne[1], B.Kharraja[1], C.W.Beausang[2], F.A.Beck[1], Th.Byrski[1], D.Curien[1], P.Dagnall[2], S.Flibotte[1], P.D.Forsyth[2], G.de France[1], B.Haas[1], A.Kiss[3], J.C.Merdinger[1], D.Prévost[1], C.Schück[4], C.Theisen[1], P.J.Twin[2], J.P.Vivien[1]

[1] *Centre de Recherches Nucléaires, IN2P3-CNRS/Université Louis Pasteur, F-67037 Strasbourg Cedex 2, France*

[2] *Oliver Lodge Laboratory, University of Liverpool, Liverpool L69 3BX, United Kingdom*

[3] *Institute of Nuclear Research, Bem tér 18/c, H-4001 Debrecen PF51, Hungary*

[4] *Centre de Spectrométrie Nucléaire et de Spectrométrie de Masse, IN2P3-CNRS, F-91405 Orsay, France*

Submitted to Nuclear Physics A

CENTRE DE RECHERCHES NUCLEAIRES
STRASBOURG

IN2P3
CNRS

UNIVERSITE
LOUIS PASTEUR

Detailed level scheme of ^{151}Tb and the feeding of the normal-deformed states by the superdeformed bands

C.M.Petrache[1,*], G.Duchêne[1], B.Kharraja[1], C.W.Beausang[2], F.A.Beck[1], T.Byrski[1], D.Curien[1], P.Dagnall[2], S.Flibotte[1], P.D.Forsyth[2], G.de France[1], B.Haas[1], A.Kiss[3], J.C.Merdinger[1], D.Prévost[1], C.Schück[4], C.Theisen[1], P.J.Twin[2], J.P.Vivien[1],

[1] *Centre de Recherches Nucléaires, Institut National de Physique Nucléaires et de Physique des Partiques, Centre National de la Recherche Scientifique, Université Louis Pasteur, F-67037 Strasbourg Cedex, France*

[2] *Oliver Lodge Laboratory, University of Liverpool, Liverpool L69 3BX, United Kingdom*

[3] *Institute of Nuclear Research, Bem tér 18/c, H-4001 Debrecen PF51, Hungary*

[4] *Centre de Spectrométrie Nucléaire et de Spectrométrie de Masse, Institut National de Physique Nucléaire et de Physique des Particules, Centre National de la Recherche Scientifique, F-91405 Orsay, France*

Abstract

Excited states in the nucleus ^{151}Tb have been investigated up to spin 91/2 $\hbar$ and 16.5 MeV energy using the ^{130}Te(^{27}Al,6n) reaction and the EUROGAM array. The theoretical interpretation of the level scheme has been performed in the framework of the Deformed Independent Particle Model. The feeding patterns of the normal-deformed states by both the yrast and first excited superdeformed bands have also been established. The results indicate that the decay-out mechanism of the bands is not of purely statistical nature, but depends on the configurations of both normal and superdeformed states.

* On leave from Institute of Physics and Nuclear Engineering, P.O.Box MG-6, Bucharest, Romania.

1. INTRODUCTION

With the advent of the new generation of gamma-ray spectrometers (EUROGAM, GASP, GAMMASPHERE), which allow the observation of very weakly populated states at low spin, yrare states well above the yrast line and very high spin states, a detailed analysis of nuclear level schemes is now possible. This opens the way to the search for the linking transitions between the superdeformed (SD) bands and the normal-deformed states, which would help to fix the band-head spin and excitation energy of the SD bands and consequently to firmly assign spins, excitation energies and specific nucleonic configurations to those structures. Up to now only in two cases of highly deformed bands in the A=130 mass region have such linking transitions been firmly established[1,2]. In this region the nucleus has prolate shape both in normal and highly deformed states, with the quadrupole deformation changing from $\beta \sim 0.2$ to $\beta \sim 0.4$. In the mass A=150 region the situation is very different: the nuclear shape changes from oblate with $\beta \sim -0.1$ to superdeformed prolate with $\beta \sim 0.6$. It is not clear if the decay out of the SD bands proceeds through many intermediate states and yet unobserved transitions, but indications exist about the spread of the final decay over many yrast and yrare normal-deformed states[3]. It appears that the task of finding linking transitions in this mass region can only be accomplished with very powerful spectrometers and with a detailed knowledge of the normal-deformed level scheme.

In the present work we have developed the level scheme of ^{151}Tb up to very high spin and excitation energy, due to the high resolving power of the EUROGAM array. We have also established the feeding patterns of the states in the first minimum fed by the yrast and first excited SD bands.

The low and medium spin levels of ^{151}Tb have been previously studied using the ^{151}Eu(α,4n), ^{151}Eu(^{3}He,3n) reactions[4] and the high spin levels up to 77/2 $\hbar$ using the ^{124}Sn(^{31}P,4n) reaction[5].

2. EXPERIMENTAL METHODS AND RESULTS

The gamma decay of the excited states in ^{151}Tb has been investigated using the EUROGAM spectrometer built by a joint France-UK collaboration [6,7]. It consists of 45 large volume germanium detectors (42 were operational in this experiment) of $\geq$ 70% relative efficiency (compared to a 3 in $\times$ 3 in NaI) at a γ-ray energy of 1.33 MeV. The array has a full energy peak efficiency of $\approx$ 4.5%. Each detector is surrounded by bismuth germanate scintillators to efficiently suppress the Compton background leading to a peak-to-total ratio of about 0.55 with a ^{60}Co source. The experiment was carried out at the

Daresbury Nuclear Structure Facility. The ^{151}Tb nucleus was populated via the heavy-ion fusion-evaporation reaction ^{130}Te(^{27}Al,6n) at a bombarding energy of 154 MeV. The target of 550 μg.cm^{-2} thickness was evaporated onto a 440 μg.cm^{-2} gold foil facing the beam so that ^{151}Tb nuclei were recoiling in vacuum. The counting rates in the individual germanium detectors were about 8 kHz. Unsuppressed events with a γ-ray multiplicity of at least 7 were required, leading to a mean multiplicity value of 3.9 after Compton suppression. A data set of 5.5 $\times$ 10^8 suppressed events was recorded during 80 hours of beam time. The unpacking of these high-fold events produced 4.6 $\times$ 10^9 gamma coincidences of order 3 and 3.1 $\times$ 10^9 coincidences of order 4.

The combined effects of high statistics and efficiency for high fold coincidences allowed the observation of very weak gamma transitions, of the order of 10^{-3} compared to the most intense transition in the nucleus. The large number of coincidences of order 3 offered the possibility to generate single-gated $\gamma\gamma$ coincidence matrices with sufficient statistics and it was therefore possible to study events in coincidence with specific γ-ray transitions in various parts of the level scheme.

Such a $\gamma\gamma$ matrix in coincidence with the 615.9, 682.7, 178.4 and 194.7 keV transitions of the negative parity band was used to reveal the higher members of this band and its connections with other structures in the nucleus (see fig.1b and fig.2). Another matrix of events in coincidence with the 1322.4, 779.5, 637.0 and 381.4 keV transitions between positive parity states was used to extend the level scheme at higher spins and to place the new high spin yrare levels (see fig.1a and fig.2). In that way, a detailed level scheme of ^{151}Tb was constructed up to spin (91/2$^-$) and 16.5 MeV excitation energy (see fig.2). At low and medium spins, many new very weak transitions connecting the different known level sequences and also new yrare levels have been placed.

In order to assign spins and parities to the levels, the data were sorted to allow a γ-ray angular distribution analysis. The Ge counters were distributed in rings as follows: 9 detectors at 72°, 4 at 86°, 4 at 94°, 10 at 108°, 10 at 133° and 5 at 157° with respect to the beam axis. In order to avoid contaminants from nearby nuclei or from multiplets in the same nucleus, we constructed sets of six spectra corresponding to the six rings, double-gated with pairs of carefully selected γ rays from the main yrast cascade as well as from the negative parity sequence of ^{151}Tb.

Taking into account that there is no evidence for isomers with a half-life longer than $\sim$4 ns up to the highest spins which could possibly decay via M2 (magnetic quadrupole) or higher order multipolarity transitions, nearly all ΔI=2 transitions were assumed to have E2 character. For the ΔI = 1 transitions, only theoretical considerations which favor one or another configuration were used in order to propose parity assignments to

the corresponding levels.

The information about γ-ray energies, intensities, angular distribution coefficients and spin-parity assignments are summarized in table 1. The detailed level scheme is presented in figure 2.

3. THE LEVEL SCHEME OF ^{151}Tb

The major part of the level scheme established in the present work is in agreement with previous studies [4,5]. The high sensitivity of the EUROGAM array enabled the observation and placing of new transitions and changes in the assignment of some γ-rays. New weak transitions in the lower spin part of the decay scheme include weak branches (146.0 and 339.8 keV γ-rays) connecting the $33/2^+$ and $37/2^+$ levels respectively with the negative parity sequence, and the 423.5 keV transition which populates the $21/2^+$ state. These transitions were extremely useful for assigning spins and parities to the various states. An important change with respect to the high spin levels reported in ref. 5 is that the 381.4 keV transition in the main positive parity sequence has been placed at a higher spin and excitation energy (deexcitation of the $61/2^+$ state). This was established due to the much higher statistics of the present experiment, which enabled the observation of the very weak transitions of 282.8 and 653.2 keV connecting the $57/2^+$ state to the $(55/2^+)$ and $53/2^-$ states, and the transitions of 670.8 and 710.4 keV connecting the two $53/2^+$ states to the $51/2^-$ negative parity state.

The low spin negative parity sequence has been developed up to the $51/2^-$ yrast state and the ordering of the levels is fixed by the presence of connecting transitions to the neighbouring yrare or yrast levels. As compared with ref.5, the higher spin negative parity sequence 368.2, 427.8, 205.8, 919.9 and 321.4 keV , was rearranged and connected with the positive parity levels.

Many new γ-ray lines with energies around 1 MeV which feed the $61/2^+$ level have been observed in the present work and this is a possible consequence of a drastic change in configuration, as will be discussed later. Above spin $67/2^-$, apart from the yrast sequence we identified many other levels, connected by rather high energy gamma transitions. Since the intensities of those transitions were usually ≤ 1 % from the total population of the 6n reaction channel, it was not possible to measure their angular distributions and therefore to assign spins to the corresponding levels.

4. DISCUSSION

The level scheme of ^{151}Tb was interpreted by means of a Deformed Independent Particle Model (D.I.P.M.)[8] which is an improved version of the model presented in ref.9,

involving a deformed single particle field and a monopole pairing interaction treated by particle-number projection. The non-spherical component of the single particle field is that of a Nilsson Hamiltonian, while the main spherical single particle energies are extracted from binding energies and spectroscopic data originating from single particle stripping and pick-up reactions. The total energy is calculated with a particle number projected B.C.S. wave function and renormalized according to the Strutinsky prescription. The configuration assignment for the main experimental levels are given in table 2. For a level with given spin and parity, the calculated configurations with the lowest excitation energy have been usually adopted. Whenever more than one configuration with similar excitation energies are predicted for a given level, making meaningless the lowest excitation energy criterion, the decay modes of the specific level have been analysed and the configurations which favour the most intense observed transitions have been adopted. The comparison with the ^{150}Gd isotone[10] shown in figure 4, together with the configurations calculated with the same model (D.I.P.M.), provides further strong support to the suggested configurations, taking into account the fact that most of the levels in ^{151}Tb can be explained assuming a $h_{11/2}$ proton coupled to the ^{150}Gd core.

4.1. The low-spin states

The nucleus ^{151}Tb has one proton and four neutrons outside the Z=64, N=82 ^{146}Gd closed shell spherical nucleus. The lowest available shell-model orbitals are $s_{1/2}$,$d_{3/2}$ and $h_{11/2}$ for protons and $f_{7/2}$,$h_{9/2}$ and $i_{13/2}$ for neutrons.

The low lying levels above the $11/2^-$ isomer can be interpreted as members of the quasi-particle multiplets with the odd proton in the $h_{11/2}$ orbital and the four valence neutrons excited in the lowest available orbitals ($f_{7/2}$, $h_{9/2}$, $i_{13/2}$). As a result of the octupole vibrations in the isotone ^{150}Gd[11], the lowest states are also expected to contain in their wave functions a considerable amount of collective vibrations. As the theoretical calculations with DIPM consider only the quasi-particle contribution, the corresponding levels are predicted at too high energies relative to experiment. However, it is well established[12] that when including the coupling of the $h_{11/2}$ proton with the 3^- octupole phonon one obtains a sizeable lowering of the corresponding level energies. Therefore, for the low spin states up to $45/2^+$ on the positive parity cascades and up to $35/2^-$ on the negative parity sequence, we adopted the same configurations as proposed by Kemnitz et al. in ref. 4, with the odd proton in the $h_{11/2}$ orbital (coupled to the 3^- octupole phonon for most of the positive parity states) and the neutrons in the above mentioned lowest available orbitals (see table 2).

4.2. The high spin states

Above the $49/2^+$ state on the positive parity side and the $39/2^-$ one on the negative parity side, one can generate higher spins either by exciting the four valence neutrons and aligning their angular momenta along the symmetry axis or by breaking the proton core. For the positive parity states, which also constitute the yrast sequence, all the states up to spin $61/2^+$ have four active neutrons and a $\pi(d_{5/2}^{-1}h_{11/2}^2)$ proton configuration, apart from the peculiar $49/2^+$ state which has two of the four valence neutrons coupled to 0 and two $d_{5/2}$ proton holes also coupled to 0. For the negative parity states, there are often two levels with the same spin. After a careful analysis of the interconnecting γ-ray transitions, assuming that the decay from one state to another involves single nucleonic rearangements, we suggest for most of the levels with spins between $43/2_1^-$ and $61/2^-$ configurations based on 4 valence neutrons in the $f_{7/2}$, $h_{9/2}$ or $i_{13/2}$ orbitals and a broken proton core, with a hole in the $d_{5/2}$ or $g_{7/2}$ orbitals and 2 particles in the $h_{11/2}$ orbital. The remaining negative parity states in this spin range, i.e. $43/2_2^-$, $45/2_1^-$, $47/2^-$, $(49/2^-)$, $51/2_1^-$, have not a broken proton core, but gain spin by promoting two of the valence neutrons in the $i_{13/2}$ orbital.

The presence of many transitions with energies $E_\gamma > 1$ MeV feeding the $61/2^+$ level, is a clear indication that to generate higher angular momentum another proton must be promoted from the core. Indeed, the main part of the yrast and yrare levels with spins between $63/2^-$ and $79/2^-$ can be well interpreted by four valence neutrons in the $f_{7/2}$, $h_{9/2}$, $i_{13/2}$ orbitals coupled to two protons from the core (see table 2). Only for the $65/2^+$ state, decaying mainly through the 1096 keV transition, a mixed configuration between the $\nu(f_{7/2}^2 h_{9/2} i_{13/2}) \otimes \pi(d_{5/2}^{-2} h_{11/2}^3)$ and $\nu(f_{7/2} h_{9/2} i_{13/2}^2) \otimes \pi(d_{5/2}^{-1} h_{11/2}^2)$ makes probably a difference. A similar assignment was done also to the $61/2^+$ isomer in ^{149}Tb[13].

The yrast states above spin $79/2^-$ and some yrare states above spin $75/2^-$ can be obtained only by breaking the N=82 neutron core and promoting the odd neutron in the $f_{7/2}$, $h_{9/2}$ and $i_{13/2}$ orbitals.

As a general comment concerning the configuration assignments, we can say that most of the yrast states correspond to maximum aligned angular momenta states and the calculated oblate deformation increases slowly with excitation energy and spin from $\beta \simeq$-0.05 up to$\beta \simeq$ - 0.20 (see table 2).

5. THE DECAY-OUT OF THE YRAST AND FIRST EXCITED SD BANDS

During the analysis special attention has been paid to the transitions which are in coincidence with the yrast and first excited SD bands [14,15]. The other six excited SD bands recently discovered in ^{151}Tb are too weak to allow such an analysis[16].

The observed decays-out of the yrast and first excited SD bands are very different. Whereas the yrast SD band deexcites at an angular momentum $I = 32.5\hbar$, the first excited band surprisingly decays-out at a lower angular momentum $I = 26.5\hbar$[15]. This effect has been attributed to differences in high-N intruder configurations and pairing correlations between the two bands. The relative population by the SD bands of the normal-deformed states in ^{151}Tb are given in table 3. Spectra gated by all pairs of transitions in the SD bands are shown in fig.3, where only γ rays deexciting higher lying normal-deformed states are indicated.

The results of the present work show that the yrast SD band feeds yrast and yrare states of both positive and negative parity, with spins between 45/2 and 63/2, with an average entry spin of $\langle J \rangle = 27.5$. In contrast, the first excited SD band feeds only four positive parity yrast states, with spins between $35/2^+$ and $45/2^+$ ($\langle J \rangle = 20.5$). The difference of $\sim 7\hbar$ between the two average entry spins into states of the first minimum is consistent with the later decay-out of the first excited SD band in ^{151}Tb[15]. One observes also that both the yrast and first excited bands have spin differences of $\sim 6\hbar$ if one assumes the proposed spins of Ragnarsson[18] for the SD bands. This large difference suggests that the deexcitation cascades have at least 3 unobserved transitions.

The intriguing question arises why does the first excited SD band lying >500 keV above the yrast SD band[15] feeds only four normal-deformed states all of positive parity, while the yrast band feeds many more normal-deformed states of both parities? It seems that the deexcitation process is not purely statistical and preferes certain "classes of states". It appears also that the final states have to remember the specific configurations of the SD bands to which they are connected, otherwise one could hardly explain the selectivity in populating states of only positive parity.

In the coincident spectrum with the yrast SD band members, weak transitions which connect yrare negative parity levels are strongly enhanced, e.g. the $166.6(47/2^- \rightarrow 45/2^-)$, $343.9(45/2^- \rightarrow 43/2^-)$, $428.6(55/2^- \rightarrow 53/2^-)$, $368.2(53/2^- \rightarrow 51/2^-)$, $205.8(57/2^- \rightarrow 55/2^-)$, $322.3(55/2^+ \rightarrow 53/2^-)$, $321.4(63/2^- \rightarrow 61/2^-)$ keV transitions. This implies that the feeding of the yrare normal-deformed states is strongly enhanced when populated by the SD band as compared to the population by the normal-deformed very high spin states. Taking the previous configuration assignments for the levels fed by the SD bands, one observes that nearly all states have two neutrons in the $i_{13/2}$ orbital. Hence, the decay out of this particular SD band for which the high-N intruder $\pi 6^3 \nu 7^2$ configuration has been assigned[14], turns out to preferentially feed some specific normal-deformed states with two neutrons in the $i_{13/2}$ orbital, giving an indication that the mixing between the SD band with the normal deformed states in which they are embedded[17] could have an

important $(i_{13/2})^2$ neutron component.

The complexity of the decay out of the yrast SD band and the insufficient statistics are two limitations we encountered in the search for linking transitions in the nucleus ^{151}Tb. The higher efficiency, resolution and sensitivity of EUROGAM Phase 2 will allow to decrease the limit of sensitivity to less than 10^{-5} and therefore, hopefully, enable us to identify the various pathways between the two extreme structures.

6. CONCLUSIONS

In this work we have established the decay scheme of ^{151}Tb up to very high spin (91/2) and excitation energy (16.5 MeV). Configurations in terms of spherical single particle orbitals have been suggested for most observed states. The decay out study of the yrast and first excited SD bands indicates that the yrast SD band feeds normal-deformed states of both parities with an average angular momentum of $\sim 27.5\hbar$ whereas the excited band feeds states of only positive parity at a lower average spin of $\sim 20.5\hbar$. We have not observed linking transitions between the SD and normal-deformed states but hopefully the future arrays, with an improved sensitivity, will enable us to identify individual decay pathways feeding the normal-deformed states.

EUROGAM is founded jointly by the SERC(U.K.) and IN2P3(France). We thank E.V.Iacob who provided the angular distribution computer code together with useful explanations.

REFERENCES

[1] E.M. Beck, F.S. Stephens, J.C. Bacelar, M.A. Deleplanque, R.M. Diamond, J.E. Draper, C. Duyar, R.J. McDonald, Phys. Rev. Lett. **58** (1987)2182

[2] D. Bazzacco, F. Brandolini, R. Burch, A. Buchemi, C. Cavedon, D. De Acuna, S. Lunardi, R. Menegazzo, P. Pavan, C. Rossi-Alvarez, M. Sferrazza, R. Zanon, G. deAngelis, P. Bezzon, M.A. Cardona, M. De Poli, G. Maron, M.L. Mazza, D. Napoli, J. Rico, P. Spolaore, X.N. Tang, G. Vedovato, N. Blasi, I. Castiglioni, G. Falconi, G. LoBianco, P.G. Bizzeti, R. Wyss, Phys. Lett. **B309** (1993)235

[3] A. Ataç, M. Piiparinen, B. Herskind, J. Nyberg, G. Sletten, G. deAngelis, S. Forbes, N. Gjørup, G. Hagemann, F. Ingebretsen, H. Jensen, D. Jerrestam, H. Kusakari, R.M. Lieder, G.V. Marti, S. Mullins, D. Santonocito, H. Schnare, K. Strähle, M. Sugawara, P.O. Tjøm, A. Virtanen, R. Wadsworth, Phys. Rev. Lett. **70** (1993)1069

[4] P. Kemnitz, L. Funke, F. Stary, E. Will, G. Winter, S. Elfström, S.A. Hjorth, A. Johnson, Th. Lindblad, Nucl. Phys. **A311** (1978)11

[5] D. Curien, Ph.D. Thesis, U.L.P. Strasbourg (1988)

[6] F.A. Beck, Prog. Part. Nucl. Phys. **28** (1992)443

[7] C.W. Beausang, S.A. Forbes, P. Fallon, P.J. Nolan, P.J. Twin, J.N. Mo, J.C. Lisle, M.A. Bentley, J. Simpson, F.A. Beck, D. Curien, G. deFrance, G. Duchêne, D. Popescu, Nucl. Instr. and Meth.**A313**(1992)37

[8] T. Døssing, K. Neergård and H. Sagawa, Phys. Scr. **24** (1981)258

[9] K. Matsuyanagi, T. Døssing and K. Neergård, Nucl. Phys. **A307** (1978)253

[10] P. Fallon, Ph.D. Thesis, Oliver Lodge Lab., Univ. of Liverpool (1989)

[11] D.R. Haenni, T.T. Sugihara, Phys. Rev. **C 16** (1977)120

[12] M. Lach, P. Kleinheinz, M. Piiparinen, M. Ogawa, S. Lunardi, M.C. Bosca, J. Styczen, J. Blomqvist, Z. Phys. **A341** (1991)25

[13] Z. Meliani, J.S. Dionisio, C. Schück, Ch. Vieu, F.A. Beck, T. Byrski, D. Curien, G. Duchêne, J.C. Merdinger, P. Fallon, J.W. Roberts, J.F. Sharpey-Schafer, to be published in Nucl. Phys. A

[14] T. Byrski, F.A. Beck, D. Curien, C. Schück, P. Fallon, A. Alderson, I. Ali, M.A. Bentley, A.M. Bruce, P.D. Forsyth, D. Howe, J.W. Roberts, J.F. Sharpey-Schafer, G. Smith, P.J. Twin, Phys. Rev. Lett. **64** (1990)1650

[15] D. Curien, G.de France, C.W. Beausang, F.A. Beck, T. Byrski, S. Clarke, P. Dagnall, G. Duchêne, S. Flibotte, S. Forbes, P.D. Forsyth, B. Haas, M.A. Joyce, B. Kharraja, B.M. Nyako, C. Schück, J. Simpson, C. Theisen, P.J. Twin, J.P. Vivien, L. Zolnai, Phys. Rev. Lett. **71** (1993)2559

[16] B. Kharraja et al, to be published

[17] E. Vigezzi, R.A. Broglia, T. Døssing, Phys. Lett. **B249** (1990)163

[18] I. Ragnarsson, Nucl.Phys. **A557** (1993)167c

Figure Captions

Figure 1. Total projections of single-gated $\gamma\gamma$ coincidence matrices: a) gates on transitions between the highest positive parity states and b) gates on transitions between low spin negative parity states.

Figure 2. Level scheme of ^{151}Tb (only the level scheme above the $11/2^-$ isomer is presented).

Figure 3. Double gated spectra with all pairs of γ rays in the: a) yrast SD band and b) first excited SD band. The highest normal-deformed coincident transitions are indicated by their energies, whereas the lowest members of the SD bands are indicated by stars.

Figure 4. Comparison between the experimental levels in the isotones ^{151}Tb and ^{150}Gd with the calculated values by the DIPM model[8,9]. Only strongly populated states in heavy-ion fusion reaction are shown. The negative (positive) parity states in ^{151}Tb are compared to positive (negative) parity states in ^{150}Gd in figure 4a (4b), respectively. In the upper part of figure 4b the highest negative parity yrast levels of ^{151}Tb are also shown. Dotted lines connect levels in ^{151}Tb having one $h_{11/2}$ proton in addition to the ^{150}Gd calculated (with the same DIPM model) configurations. The orbitals involved in the assigned configurations are shown in the right part of the pannels (see also table 2).

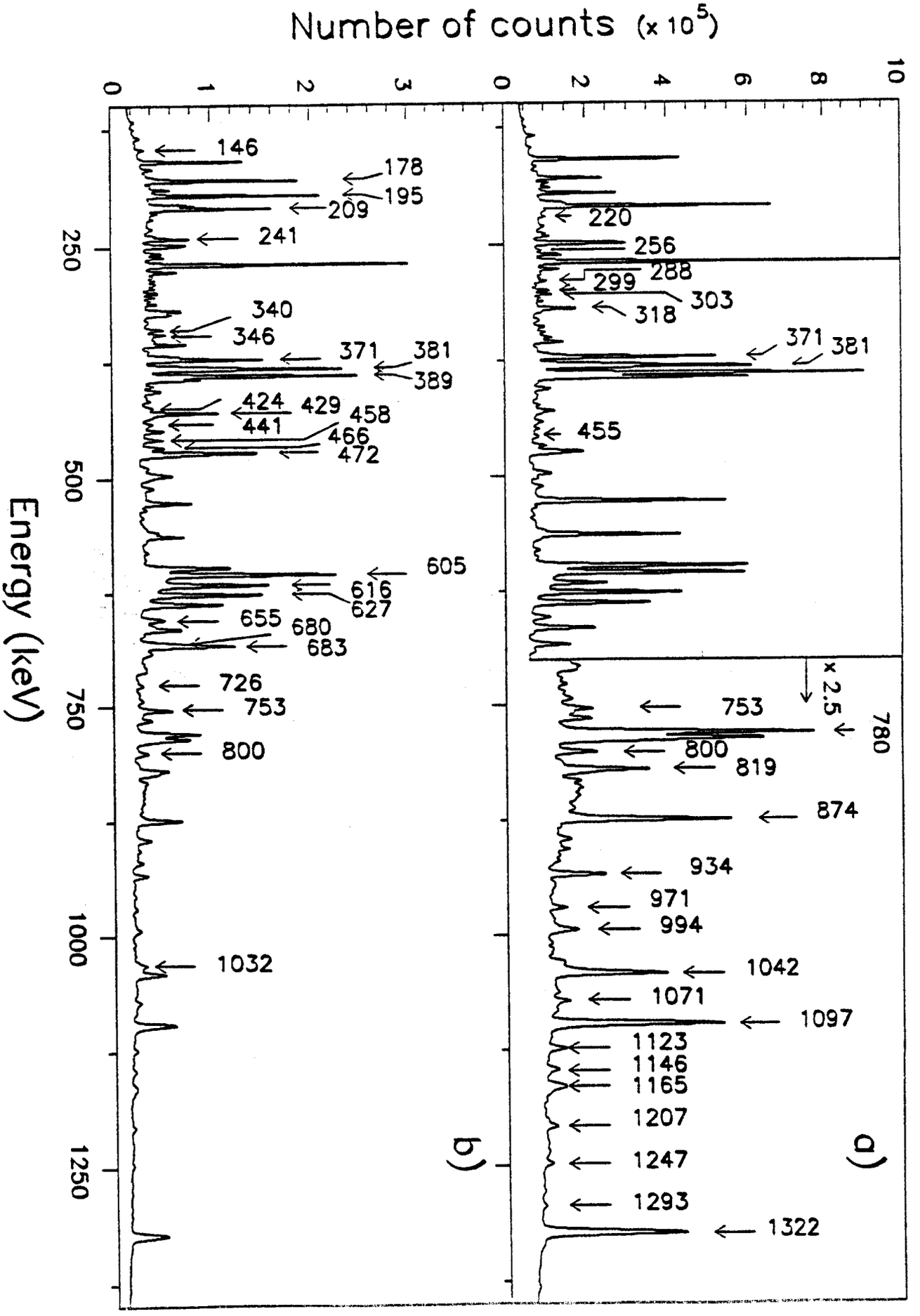
Number of counts (x 10^5)
Energy (keV)
a)
b)
× 2.5
146
178
195
209
241
340
346
371
381
389
424
429
441
458
466
472
605
616
627
655
680
683
726
753
800
1032
220
256
288
299
303
318
371
381
455
753
780
800
819
874
934
971
994
1042
1071
1097
1123
1146
1165
1207
1247
1293
1322

Figure 1.

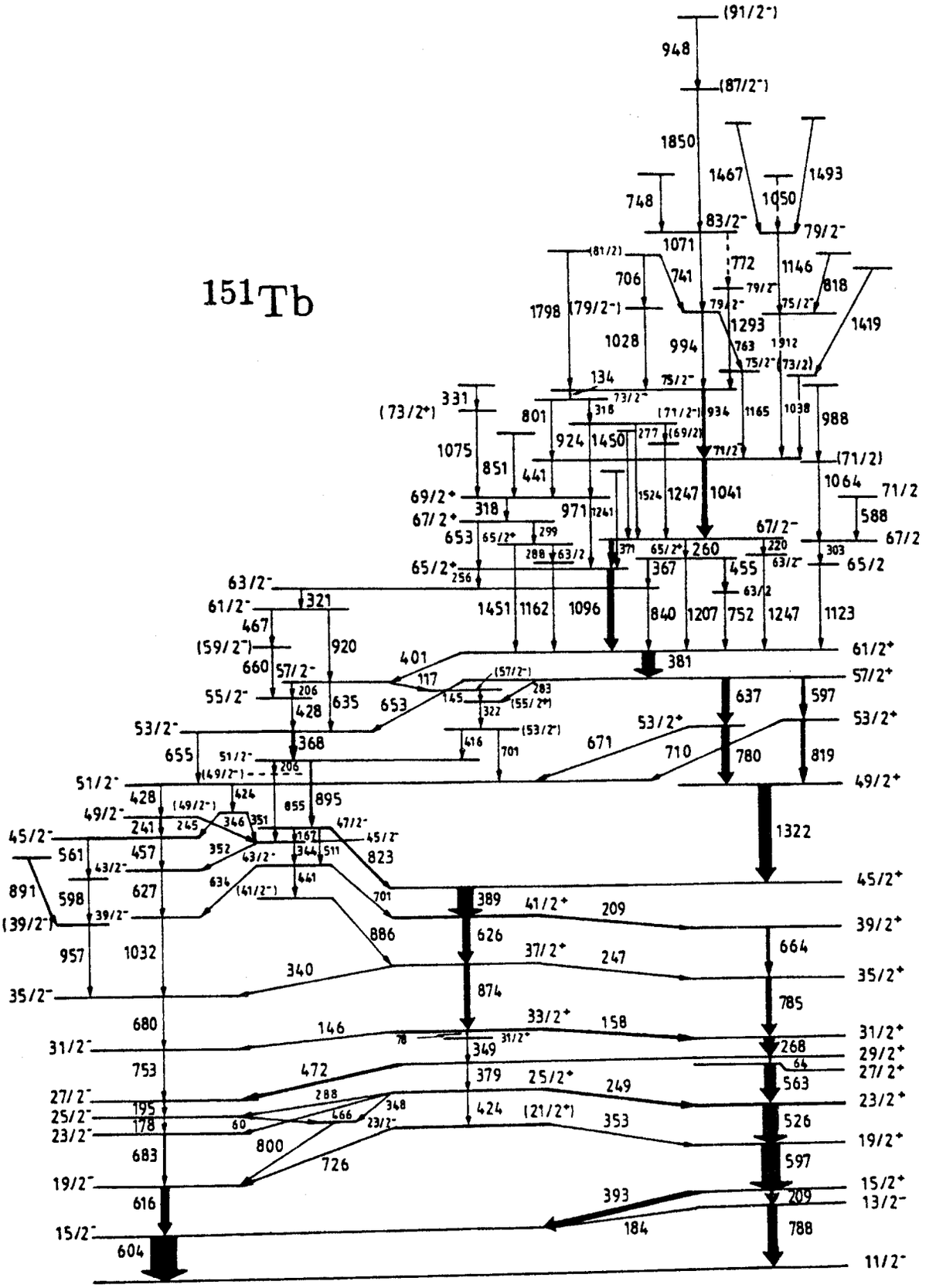
151Tb
(91/2⁻)
948
(87/2⁻)
1850
1467
1493
748
1050
83/2⁻
79/2⁻
1071
(81/2)
772
1146
706
741
818
1798
(79/2⁻)
1293
1419
1028
994
763
1912
134
331
(73/2⁺)
801
318
(71/2⁻)
934
1165
1038
988
924
1450
277
(69/2)
1075
851
441
(71/2)
1064
71/2
69/2⁺
318
971
1241
1524
1247
1041
588
67/2⁺
653
299
67/2⁻
67/2
65/2⁺
288
63/2
371
260
220
303
65/2
256
367
455
63/2
63/2⁻
321
1451
1162
1096
840
1207
752
1247
1123
61/2⁻
467
(59/2⁻)
920
401
381
61/2⁺
660
57/2⁻
117
(57/2⁻)
57/2⁺
206
283
55/2⁻
428
635
653
145
(55/2⁻)
637
597
322
53/2⁻
(53/2⁻)
53/2⁺
53/2⁺
655
368
416
671
710
780
819
51/2⁻
701
(49/2⁻)
206
49/2⁺
428
424
895
855
49/2⁻
(49/2⁻)
241
245
346
351
47/2⁻
1322
45/2⁻
167
45/2⁻
561
457
352
43/2⁻
344
511
823
45/2⁺
43/2⁻
891
598
627
634
(41/2⁻)
441
701
389
41/2⁺
209
(39/2⁻)
39/2⁻
39/2⁺
886
626
664
957
1032
37/2⁺
247
340
35/2⁺
35/2⁻
874
785
680
146
33/2⁺
158
31/2⁺
31/2⁻
78
31/2⁺
349
268
29/2⁺
753
472
379
25/2⁺
64
27/2⁺
27/2⁻
249
563
288
195
348
23/2⁺
25/2⁻
60
466
424
(21/2⁺)
353
526
178
23/2⁻
23/2⁻
19/2⁺
800
683
597
726
19/2⁻
15/2⁺
393
209
616
13/2⁻
184
788
15/2⁻
604
11/2⁻

Figure 2.

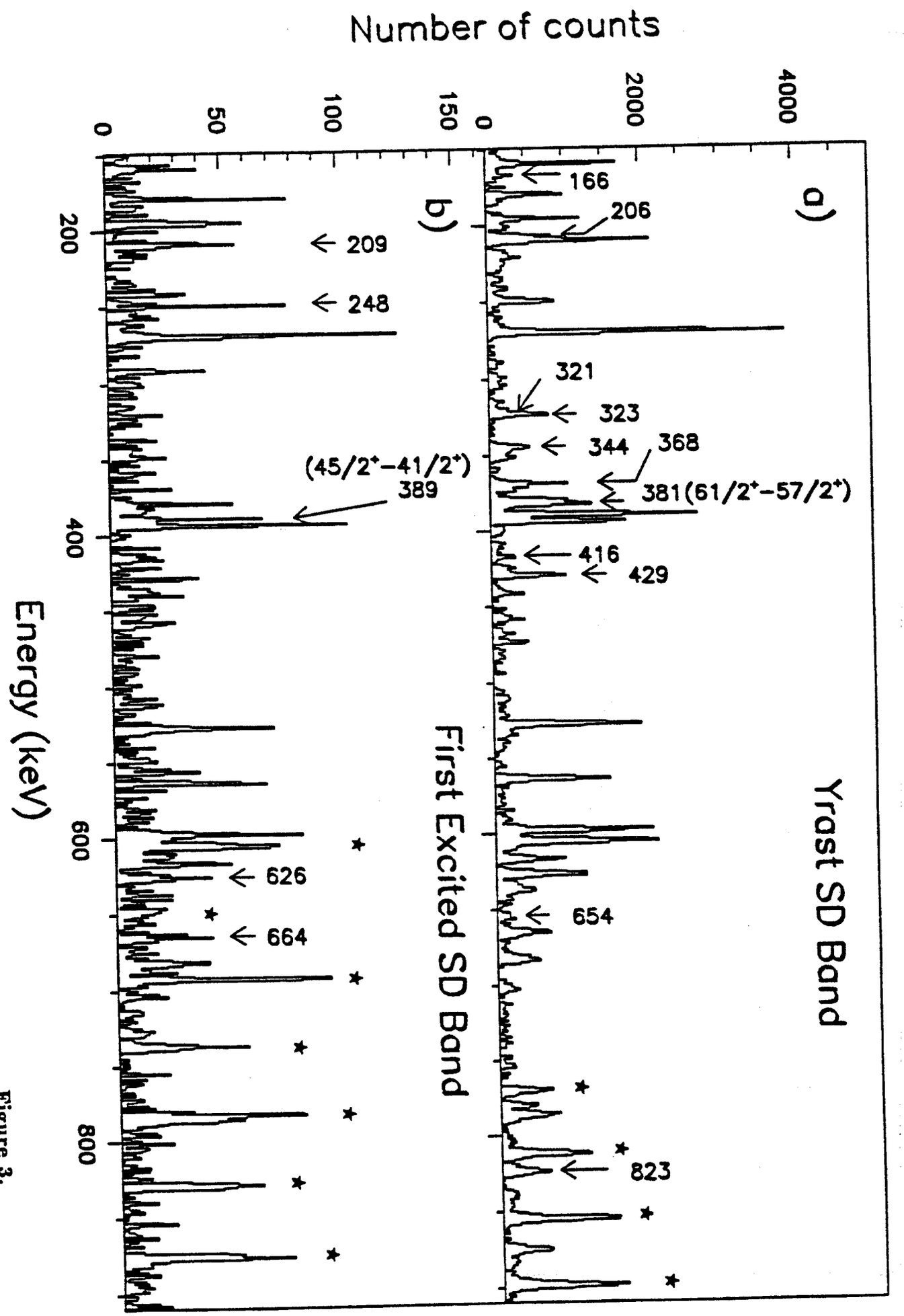
Number of counts
0
50
100
150
0
2000
4000
b)
a)
166
206
209
248
321
323
344
368
(45/2⁺–41/2⁺)
389
381(61/2⁺–57/2⁺)
416
429
654
626
664
823
200
400
600
800
Energy (keV)
First Excited SD Band
Yrast SD Band

Figure 3.

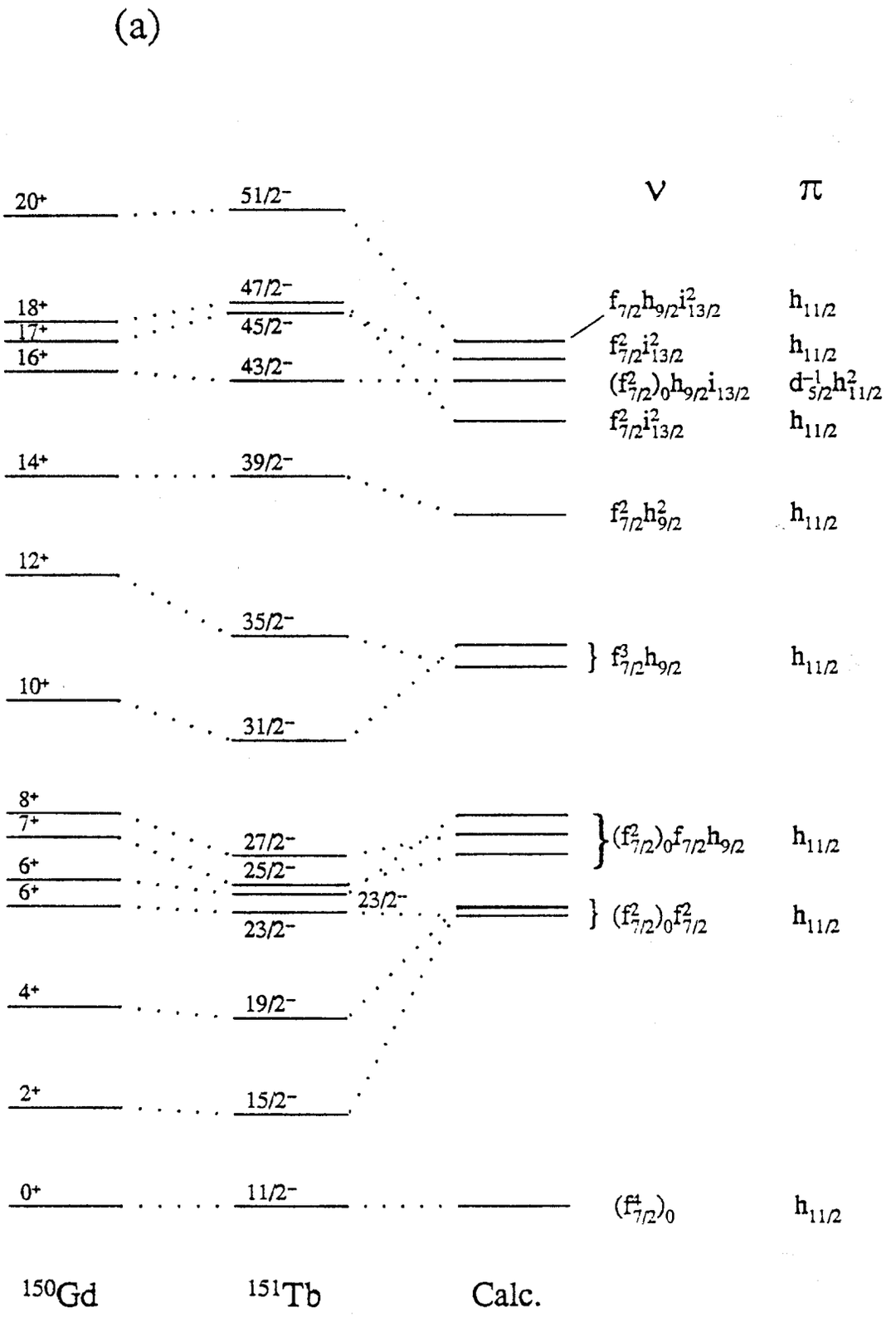
(a)
ν
π
20+
51/2−
47/2−
18+
45/2−
17+
16+
43/2−
14+
39/2−
12+
35/2−
10+
31/2−
8+
7+
27/2−
6+
25/2−
6+
23/2−
23/2−
4+
19/2−
2+
15/2−
0+
11/2−
$f_{7/2}h_{9/2}i^2_{13/2}$ $h_{11/2}$
$f^2_{7/2}i^2_{13/2}$ $h_{11/2}$
$(f^2_{7/2})_0h_{9/2}i_{13/2}$ $d^{-1}_{5/2}h^2_{11/2}$
$f^2_{7/2}i^2_{13/2}$ $h_{11/2}$
$f^2_{7/2}h^2_{9/2}$ $h_{11/2}$
} $f^3_{7/2}h_{9/2}$ $h_{11/2}$
} $(f^2_{7/2})_0f_{7/2}h_{9/2}$ $h_{11/2}$
} $(f^2_{7/2})_0f^2_{7/2}$ $h_{11/2}$
$(f^4_{7/2})_0$ $h_{11/2}$
^{150}Gd
^{151}Tb
Calc.

Figure 4.

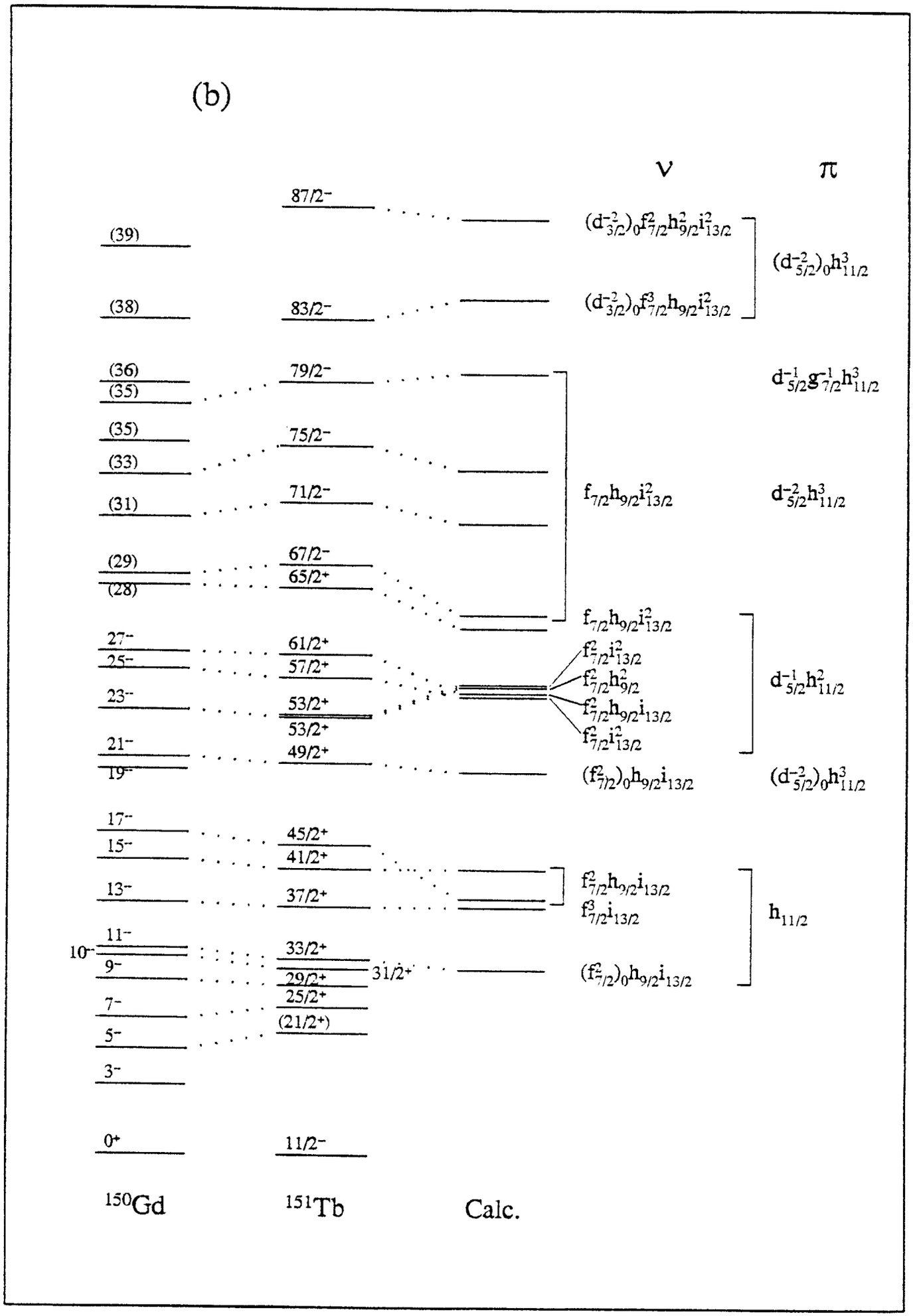
(b)
ν
π
87/2⁻
(39)
$(d^{-2}_{3/2})_0 f^2_{7/2} h^2_{9/2} i^2_{13/2}$
$(d^{-2}_{5/2})_0 h^3_{11/2}$
(38)
83/2⁻
$(d^{-2}_{3/2})_0 f^3_{7/2} h_{9/2} i^2_{13/2}$
(36)
79/2⁻
$d^{-1}_{5/2} g^{-1}_{7/2} h^3_{11/2}$
(35)
(35)
75/2⁻
(33)
$f_{7/2} h_{9/2} i^2_{13/2}$
(31)
71/2⁻
$d^{-2}_{5/2} h^3_{11/2}$
(29)
67/2⁻
(28)
65/2⁺
$f_{7/2} h_{9/2} i^2_{13/2}$
27⁻
61/2⁺
$f^2_{7/2} i^2_{13/2}$
25⁻
57/2⁺
$f^2_{7/2} h^2_{9/2}$
$d^{-1}_{5/2} h^2_{11/2}$
23⁻
53/2⁺
$f^2_{7/2} h_{9/2} i_{13/2}$
53/2⁺
$f^2_{7/2} i^2_{13/2}$
21⁻
49/2⁺
19⁻
$(f^2_{7/2})_0 h_{9/2} i_{13/2}$
$(d^{-2}_{5/2})_0 h^3_{11/2}$
17⁻
45/2⁺
15⁻
41/2⁺
$f^2_{7/2} h_{9/2} i_{13/2}$
13⁻
37/2⁺
$f^3_{7/2} i_{13/2}$
$h_{11/2}$
11⁻
10⁻
33/2⁺
9⁻
31/2⁺
29/2⁺
$(f^2_{7/2})_0 h_{9/2} i_{13/2}$
7⁻
25/2⁺
(21/2⁺)
5⁻
3⁻
0⁺
11/2⁻
150Gd
151Tb
Calc.

Figure 4.

Table 1

Gamma-ray energies, relative intensities, angular distribution coefficients[a] and spin-parity assignments for the transitions in ^{151}Tb.

E_γ(keV)	$I_\gamma^{b)}$	a_2	$I_i^\pi \rightarrow I_f^{\pi c)}$
59.7			$25/2^- \rightarrow 23/2^-$
64.2			$29/2^+ \rightarrow 27/2^+$
77.5			$33/2^+ \rightarrow 31/2^+$
117.2	0.1		$57/2^- \rightarrow (57/2^-)$
134.3	0.1		$75/2^- \rightarrow 73/2^+$
145.1	0.20(4)		$(57/2^-) \rightarrow (55/2^+)$
146.0	0.2		$33/2^+ \rightarrow 31/2^-$
158.2	14.9	-0.19 ± 0.07	$33/2^+ \rightarrow 31/2^+$
166.6	0.7(4)	-0.46 ± 0.27	$47/2^- \rightarrow 45/2^-$
178.4	7.9	-0.38 ± 0.11	$25/2^- \rightarrow 23/2^-$
183.9	2.0		$13/2^- \rightarrow 15/2^-$
194.7	8.6	-0.22 ± 0.06	$27/2^- \rightarrow 25/2^-$
205.8	2.4	-0.45 ± 0.14	$57/2^- \rightarrow 55/2^-$
206.3	0.3(1)		$51/2^- \rightarrow (49/2^-)$
208.8	14.1		$41/2^+ \rightarrow 39/2^+$
209.0	22.3		$15/2^+ \rightarrow 13/2^-$
220.2	0.4	0.45 ± 0.20	$67/2^- \rightarrow 63/2^-$
240.6	1.7(4)	0.32 ± 0.07	$49/2^- \rightarrow 45/2^-$
245.3	0.1		$(49/2^-) \rightarrow 45/2^-$
247.3	4.3		$37/2^+ \rightarrow 35/2^+$
248.7	12.7	-0.12 ± 0.14	$25/2^+ \rightarrow 23/2^+$
256.2	0.8	-0.57 ± 0.40	$65/2^+ \rightarrow 63/2^-$
260.3	2.2(1.5)	-0.24 ± 0.11	$67/2^- \rightarrow 65/2^+$
268.4	46.4	-0.32 ± 0.03	$31/2^+ \rightarrow 29/2^+$
276.9	0.7		$(71/2^-) \rightarrow (69/2^-)$
282.8	0.4(2)		$57/2^+ \rightarrow (55/2^+)$
288.2	1.4(6)	-0.52 ± 0.32	$65/2^+ \rightarrow 63/2$
288.4	1.1(5)		$25/2^+ \rightarrow 25/2^-$
298.6	2.7(1.4)	-0.22 ± 0.18	$67/2^+ \rightarrow 65/2^+$
302.5	2.4(1.0)	-0.24 ± 0.07	$67/2 \rightarrow 65/2$
317.6	1.2(6)		$73/2^- \rightarrow (71/2^-)$
318.2	4.6(1.5)	-0.14 ± 0.29	$69/2^+ \rightarrow 67/2^+$
321.4	1.7	-0.49 ± 0.31	$63/2^- \rightarrow 61/2^-$
322.3	0.8(2)	-0.31 ± 0.18	$(55/2^+) \rightarrow (53/2^-)$
330.7	0.20(4)		$\rightarrow (73/2^+)$
339.8	0.5		$37/2^+ \rightarrow 35/2^-$
343.9	1.2(4)	-0.24 ± 0.26	$45/2^- \rightarrow 43/2^-$
346.4	0.6(4)		$49/2^- \rightarrow 45/2^-$
348.1	0.9(2)		$25/2^+ \rightarrow 23/2^-$
348.6	1.6		$31/2^+ \rightarrow 29/2^+$
351.1	0.10(5)		$(49/2^-) \rightarrow 45/2^-$
351.5	0.40(2)		$45/2^- \rightarrow 43/2^-$
352.8	0.80(7)		$(21/2^+) \rightarrow 19/2^+$

Table 1 — continued

E_γ(keV)	$I_\gamma^{b)}$	a_2	$I_i^\pi \rightarrow I_f^{\pi\,c)}$
366.9	0.7		$65/2^+ \rightarrow 63/2^-$
368.2	5.9	-0.33 ± 0.40	$53/2^- \rightarrow 51/2^-$
371.0	20.7	-0.25 ± 0.07	$67/2^- \rightarrow 65/2^+$
378.5	16.8	0.14 ± 0.02	$29/2^+ \rightarrow 25/2^+$
381.4	46.8	0.30 ± 0.04	$61/2^+ \rightarrow 57/2^+$
388.5	51.6	0.24 ± 0.06	$45/2^+ \rightarrow 41/2^+$
392.9	38.1	0.19 ± 0.03	$15/2^+ \rightarrow 15/2^-$
401.0	1.0	0.38 ± 0.26	$61/2^+ \rightarrow 57/2^-$
416.3	0.8(3)	-0.21 ± 0.24	$(53/2^-) \rightarrow 51/2^-$
423.5	1.6(5)		$25/2^+ \rightarrow (21/2^+)$
423.9	0.20(4)		$51/2^- \rightarrow (49/2^-)$
427.8	3.8	-0.13 ± 0.13	$55/2^- \rightarrow 53/2^-$
428.6	2.5	-0.32 ± 0.08	$51/2^- \rightarrow 49/2^-$
440.5	0.4		$43/2^- \rightarrow (41/2^-)$
441.3	0.6	-0.21 ± 0.16	$71/2^- \rightarrow 69/2^+$
455.3	0.9		$65/2^+ \rightarrow 63/2$
457.3	1.5	0.14 ± 0.14	$45/2^- \rightarrow 43/2^-$
466.0	0.50(9)		$25/2^+ \rightarrow 23/2^-$
466.8	3.2		$61/2^- \rightarrow (59/2^-)$
472.5	8.6	-0.40 ± 0.55	$29/2^+ \rightarrow 27/2^-$
510.5	1.2(7)		$47/2^- \rightarrow 43/2^-$
526.6	54.0	0.21 ± 0.01	$23/2^+ \rightarrow 19/2^+$
561.0	0.2		$45/2^- \rightarrow$
562.8	40.1	0.17 ± 0.03	$27/2^+ \rightarrow 23/2^+$
588.0	0.4	0.58 ± 0.66	$71/2 \rightarrow 67/2$
597.2	16.3		$57/2^+ \rightarrow 53/2^+$
597.4	63.6	0.13 ± 0.02	$19/2^+ \rightarrow 15/2^+$
598.2	0.2		$\rightarrow (39/2^-)$
604.5	71.4	0.07 ± 0.01	$15/2^- \rightarrow 11/2^-$
615.9	26.6	0.30 ± 0.03	$19/2^- \rightarrow 15/2^-$
625.8	35.0	0.32 ± 0.01	$41/2^+ \rightarrow 37/2^+$
627.0	2.3(9)	0.28 ± 0.04	$43/2^- \rightarrow 39/2^-$
634.0	0.4(2)		$43/2^- \rightarrow 39/2^-$
634.6	1.0(3)		$57/2^- \rightarrow 53/2^-$
637.0	32.6	0.29 ± 0.01	$57/2^+ \rightarrow 53/2^+$
652.7	3.6	-0.23 ± 0.09	$67/2^+ \rightarrow 65/2^+$
653.2	0.7(4)		$57/2^+ \rightarrow 53/2^-$
654.6	1.4		$53/2^- \rightarrow 51/2^-$
659.7	2.5		$(59/2^-) \rightarrow 55/2^-$
664.3	19.4	0.16 ± 0.01	$39/2^+ \rightarrow 35/2^+$
670.8	0.3		$53/2^+ \rightarrow 51/2^-$
679.6	3.6	0.25 ± 0.09	$35/2^- \rightarrow 31/2^-$
682.7	16.1	0.26 ± 0.09	$23/2^- \rightarrow 19/2^-$
700.7	0.8		$(53/2^-) \rightarrow 51/2^-$
701.1	2.5		$43/2^- \rightarrow 41/2^+$

Table 1 — continued

E_γ(keV)	$I_\gamma^{b)}$	a_2	$I_i^\pi \rightarrow I_f^{\pi\,c)}$
706.6	0.3(1)		$(81/2) \rightarrow (79/2^-)$
710.4	0.6		$53/2^+ \rightarrow 51/2^-$
726.0	2.8(4)		$(21/2^+) \rightarrow 19/2^-$
740.8	0.5(1)		$(81/2) \rightarrow 79/2^-$
747.7	0.1		$\rightarrow 83/2^-$
752.1	1.2	0.40 ± 0.24	$63/2 \rightarrow 61/2^+$
753.5	5.0	0.16 ± 0.05	$31/2^- \rightarrow 27/2^-$
763.0	0.8		$79/2^- \rightarrow 75/2^-$
771.8	0.2		$83/2^- \rightarrow 79/2^-$
779.5	31.7	0.30 ± 0.06	$53/2^+ \rightarrow 49/2^+$
785.2	29.8	0.28 ± 0.06	$35/2^+ \rightarrow 31/2^+$
788.4	28.6	-0.40 ± 0.15	$13/2^- \rightarrow 11/2^-$
800.3	1.3(7)		$23/2^- \rightarrow 19/2^-$
801.4	4.0	0.16 ± 0.09	$73/2^- \rightarrow 71/2^-$
818.7	0.7		$\rightarrow 75/2^-$
819.1	16.0	0.31 ± 0.02	$53/2^+ \rightarrow 49/2^+$
822.7	6.5	-0.34 ± 0.28	$47/2^- \rightarrow 45/2^+$
840.3	0.9(2)		$63/2^- \rightarrow 61/2^+$
851.4	1.1		$\rightarrow 69/2^+$
855.1	0.2		$(49/2^-) \rightarrow 45/2^-$
874.3	27.8	0.27 ± 0.07	$37/2^+ \rightarrow 33/2^+$
886.0	0.5		$(41/2^-) \rightarrow 37/2^+$
891.0	0.9		$\rightarrow (39/2^-)$
894.8	7.1	0.22 ± 0.09	$51/2^- \rightarrow 47/2^-$
919.9	0.9	0.14 ± 0.14	$61/2^- \rightarrow 57/2^-$
924.3	0.6		$(71/2^-) \rightarrow 69/2^+$
934.2	8.2	0.32 ± 0.05	$75/2^- \rightarrow 71/2^-$
947.8	0.1		$(91/2^-) \rightarrow (87/2^-)$
957.0	1.2		$(39/2^-) \rightarrow 35/2^-$
970.9	2.8	0.32 ± 0.03	$69/2^+ \rightarrow 65/2^+$
988.3	1.1(5)		$\rightarrow (71/2)$
993.6	3.8	0.28 ± 0.02	$79/2^- \rightarrow 75/2^-$
1027.8	1.6(5)		$(79/2^-) \rightarrow 75/2^-$
1031.7	2.8	0.52 ± 0.17	$39/2^- \rightarrow 35/2^-$
1038.0	0.7		$(73/2) \rightarrow 71/2^-$
1041.6	17.8	0.32 ± 0.02	$71/2^- \rightarrow 67/2^-$
1050.0	0.3		$\rightarrow 79/2^-$
1063.6	1.6(4)		$(71/2) \rightarrow 67/2$
1071.3	1.4	0.14 ± 0.14	$83/2^- \rightarrow 79/2^-$
1075.4	0.7		$(73/2^+) \rightarrow 69/2^+$
1096.5	30.7	0.30 ± 0.02	$65/2^+ \rightarrow 61/2^+$
1123.2	3.0(1.6)	0.31 ± 0.17	$65/2 \rightarrow 61/2^+$

Table 1 — continued.

E_γ(keV)	$I_\gamma^{b)}$	a_2	$I_i^\pi \rightarrow I_f^{\pi\,c)}$
1207.2	2.1(1)		$65/2^+ \rightarrow 61/2^+$
1240.8	0.4(2)		$\rightarrow 65/2^+$
1247.0	1.1(6)		$(69/2^-) \rightarrow 67/2^-$
1247.3	0.9(4)		$63/2^- \rightarrow 61/2^+$
1293.1	1.14(4)	0.14 ± 0.07	$79/2^- \rightarrow 75/2^-$
1322.4	41.8	0.28 ±0.01	$49/2^+ \rightarrow 45/2^+$
1419.3	0.4		$\rightarrow (73/2)$
1450.0	0.7(5)		$(71/2) \rightarrow 67/2^-$
1450.6	1.8(6)		$65/2^+ \rightarrow 61/2^+$
1466.5	0.3		$\rightarrow 79/2^-$
1493.0	0.2		$\rightarrow 79/2^-$
1523.9	0.20(5)		$(71/2^-) \rightarrow 67/2^-$
1798.2	0.4(2)		$\rightarrow 75/2^-$
1850.0	0.3(1)		$(87/2^-) \rightarrow 83/2^-$
1912.0	2.1(1)	0.28 ± 0.03	$75/2^- \rightarrow 71/2^-$

[a)] The a_4 coefficients are almost all equal to zero and therefore have been not included in the table.

[b)] Intensities corrected for efficiency and internal conversion, relative to the sum of the intensities of the 604.5 and 788.4 keV ground state transitions. Except where stated, the errors are less than 10 %.

[c)] The tentative parity of the states are indicated. The values for which angular distribution coefficients could not be extracted and which are not fixed by other interband transitions are given in parenthesis.

Table 2. *Single-particle configuration assignments for the high-spin states in ^{151}Tb. The spins given in parenthesis are not known experimentally. The subscripts indicate the ordering of states with the same spin and parity: 1 for the yrast configuration, 2 for the first excited configuration ... In columns 2 and 3 are given the experimental and theoretical excitation energies with respect to the $11/2^-$ state, whereas in the fourth column the theoretical quadrupole deformation is reported. The configurations including the 3^- octupole phonon vibration have been suggested by Kemnitz et al. (see ref.4).*

I^π	E_{exp} (MeV)	E_{th} (MeV)	β_2	Neutron	Proton
$11/2^-$	0.0	0.0	-0.05	$(f^4_{7/2})_0$	$h_{11/2}$
$13/2^-$	0.788	1.88	-0.04	$(f^4_{7/2})_2$	$h_{11/2}$
$15/2^-$	0.604	1.93	-0.05	$(f^4_{7/2})_2$	$h_{11/2}$
$15/2^+$	0.997			$(f^4_{7/2})_0$	$(3^- \otimes h_{11/2})_{15/2}$
$19/2^-$	1.220	1.94	-0.04	$(f^2_{7/2})_0 f^2_{7/2}$	$h_{11/2}$
$19/2^+$	1.595			$(f^4_{7/2})_2$	$(3^- \otimes h_{11/2})_{15/2}$
$(21/2^+)$	1.946			$(f^4_{7/2})_2$	$(3^- \otimes h_{11/2})_{17/2}$
$23/2^-_1$	1.903	1.88	-0.04	$(f^2_{7/2})_0 (f^2_{7/2})^{max}_6$	$(h_{11/2})^{max}_{11/2}$
$23/2^-_2$	2.020	2.54	-0.07	$(f^2_{7/2})_0 f_{7/2} h_{9/2}$	$h_{11/2}$
$23/2^+$	2.121			$(f^4_{7/2})_4$	$(3^- \otimes h_{11/2})_{15/2}$
$25/2^-$	2.081	2.28	-0.07	$(f^2_{7/2})_0 f_{7/2} h_{9/2}$	$h_{11/2}$
$25/2^+$	2.370			$(f^4_{7/2})_4$	$(3^- \otimes h_{11/2})_{17/2}$
$27/2^-$	2.276	2.41	-0.07	$(f^2_{7/2})_0 (f_{7/2} h_{9/2})^{max}_8$	$(h_{11/2})^{max}_{11/2}$
$27/2^+$	2.684			$(f^4_{7/2})_6$	$(3^- \otimes h_{11/2})_{15/2}$
$29/2^+$	2.748			$[(f^3_{7/2})_{5/2} h_{9/2}]_7$	$(3^- \otimes h_{11/2})_{15/2}$
$31/2^-$	3.029	3.65	-0.06	$f^3_{7/2} h_{9/2}$	$h_{11/2}$
$31/2^+_1$	3.017			$[(f^3_{7/2})_{7/2} h_{9/2}]_8$	$(3^- \otimes h_{11/2})_{15/2}$
$31/2^+_2$	3.097	2.72	-0.08	$(f^2_{7/2})_0 (f_{7/2} i_{13/2})^{max}_{10}$	$(h_{11/2})^{max}_{11/2}$
$33/2^+$	3.175	3.02	-0.11	$(f^2_{7/2})_0 (h_{9/2} i_{13/2})^{max}_{11}$	$(h_{11/2})^{max}_{11/2}$
$35/2^-$	3.709	3.51	-0.06	$(f^3_{7/2} h_{9/2})^{max}_{12}$	$(h_{11/2})^{max}_{11/2}$
$35/2^+$	3.802			$[(f^3_{7/2})_{11/2} h_{9/2}]_{10}$	$(3^- \otimes h_{11/2})_{15/2}$
$37/2^+$	4.049	4.06	-0.06	$f^3_{7/2} i_{13/2}$	$h_{11/2}$
$39/2^+$	4.466			$[(f^3_{7/2})_{15/2} h_{9/2}]_{12}$	$(3^- \otimes h_{11/2})_{15/2}$
$(39/2^-)$	4.666	5.05	-0.10	$(f^2_{7/2})_0 f_{7/2} i_{13/2}$	$d^{-1}_{5/2} h^2_{11/2}$
$39/2^-$	4.741	4.49	-0.07	$(f^2_{7/2} h^2_{9/2})^{max}_{14}$	$(h_{11/2})^{max}_{11/2}$
$41/2^+$	4.675	4.68	-0.09	$f^2_{7/2} h_{9/2} i_{13/2}$	$h_{11/2}$
$(41/2^-)$	4.935	5.16	-0.09	$(f^2_{7/2})_0 f_{7/2} i_{13/2}$	$d^{-1}_{5/2} h_{11/2}$
$43/2^-_1$	5.368	5.29	-0.12	$(f^2_{7/2})_0 h_{9/2} i_{13/2}$	$d^{-1}_{5/2} h^2_{11/2}$
$43/2^-_2$	5.376	5.58	-0.08	$f^2_{7/2} i^2_{13/2}$	$h_{11/2}$
$45/2^+$	5.064	4.19	-0.09	$(f^2_{7/2} h_{9/2} i_{13/2})^{max}_{17}$	$(h_{11/2})^{max}_{11/2}$
$45/2^-_1$	5.719	5.37	-0.09	$f^2_{7/2} i^2_{13/2}$	$h_{11/2}$
$45/2^-_2$	5.825	5.51	-0.12	$(f^2_{7/2})_0 (f_{7/2} i_{13/2})^{max}_{10}$	$(d^{-1}_{5/2} h^2_{11/2})^{max}_{25/2}$
$47/2^-$	5.886	5.10	-0.09	$(f^2_{7/2} i^2_{13/2})^{max}_{18}$	$(h_{11/2})^{max}_{11/2}$

Table 2 — continued

I^π	E_{exp} (MeV)	E_{th} (MeV)	β_2	Neutron	Proton
$49/2^-$	6.066	6.39	-0.08	$f^3_{7/2}i_{13/2}$	$d^{-1}_{5/2}h^2_{11/2}$
$(49/2^-)$	6.070	5.76	-0.11	$f_{7/2}h_{9/2}i^2_{13/2}$	$h_{11/2}$
$49/2^+$	6.386	6.27	-0.12	$(f^2_{7/2})_0(h_{9/2}i_{13/2})^{max}_{11}$	$(d^{-2}_{5/2})_0(h^3_{11/2})^{max}_{27/2}$
$51/2^-_1$	6.494	5.53	-0.11	$(f_{7/2}h_{9/2}i^2_{13/2})^{max}_{20}$	$(h_{11/2})^{max}_{11/2}$
$51/2^-_2$	6.781	6.76	-0.10	$f^2_{7/2}h_{9/2}i_{13/2}$	$d^{-1}_{5/2}h^2_{11/2}$
$53/2^-$	7.149	6.56	-0.10	$f^2_{7/2}h_{9/2}i_{13/2}$	$g^{-1}_{7/2}h^2_{11/2}$
$(53/2^-)$	7.195	6.99	-0.10	$f^2_{7/2}h_{9/2}i_{13/2}$	$d^{-1}_{5/2}h^2_{11/2}$
$53/2^+_1$	7.165	7.71	-0.09	$f^2_{7/2}i^2_{13/2}$	$d^{-1}_{5/2}h^2_{11/2}$
$53/2^+_2$	7.205	7.66	-0.07	$(f^2_{7/2}h^2_{9/2})^{max}_{28}$	$(d^{-1}_{5/2}h^2_{11/2})^{max}_{25/2}$
$(55/2^+)$	7.517	6.99	-0.10	$f^2_{7/2}i^2_{13/2}$	$d^{-1}_{5/2}h^2_{11/2}$
$55/2^-$	7.577	6.56	-0.10	$f^2_{7/2}h_{9/2}i_{13/2}$	$d^{-1}_{5/2}h_{11/2}$
$(57/2^-)$	7.663	7.19	-0.10	$f^2_{7/2}h_{9/2}i_{13/2}$	$g^{-1}_{7/2}h^2_{11/2}$
$57/2^-$	7.782	6.76	-0.10	$f^2_{7/2}h_{9/2}i_{13/2}$	$d^{-1}_{5/2}h^2_{11/2}$
$57/2^+$	7.802	7.51	-0.10	$f^2_{7/2}i^2_{13/2}$	$d^{-1}_{5/2}h^2_{11/2}$
$(59/2^-)$	8.236	7.76	-0.09	$f^2_{7/2}h_{9/2}i_{13/2}$	$g^{-1}_{7/2}h^2_{11/2}$
$61/2^+$	8.183	7.56	-0.10	$(f^2_{7/2}h_{9/2}i_{13/2})^{max}_{17}$	$(d^{-2}_{5/2})_0(h^3_{11/2})^{max}_{27/2}$
		7.84	-0.11	$f_{7/2}h_{9/2}i^2_{13/2}$	$d^{-1}_{5/2}h^2_{11/2}$
$61/2^-$	8.703	8.18	-0.08	$(f^2_{7/2}h_{9/2}i_{13/2})^{max}_{17}$	$(g^{-1}_{7/2}h^2_{11/2})^{max}_{27/2}$
$63/2^-_1$	9.024	8.52	-0.10	$(f^2_{7/2}i^2_{13/2})^{max}_{18}$	$(d^{-2}_{5/2})_0(h^3_{11/2})^{max}_{27/2}$
$63/2^-_2$	9.431	9.39	-0.09	$(f_{7/2}h^2_{9/2}i_{13/2})^{max}_{18}$	$(g^{-1}_{7/2}h^2_{11/2})^{max}_{27/2}$
$65/2^+_1$	9.280	8.62	-0.11	$(f_{7/2}h_{9/2}i^2_{13/2})^{max}_{20}$	$(d^{-1}_{5/2}h^2_{11/2})^{max}_{25}$
$65/2^+_2$	9.391	9.08	-0.11	$f^2_{7/2}h_{9/2}i_{13/2}$	$d^{-2}_{5/2}h^3_{11/2}$
$65/2^+_3$	9.634	9.15	-0.10	$f_{7/2}h_{9/2}i^2_{13/2}$	$g^{-1}_{7/2}h^2_{11/2}$
$67/2^-$	9.651	8.83	-0.12	$(f_{7/2}h_{9/2}i^2_{13/2})^{max}_{20}$	$(d^{-2}_{5/2})_0(h^3_{11/2})^{max}_{27/2}$
$67/2^+$	9.933	9.60	-0.09	$(f_{7/2}h_{9/2}i^2_{13/2})^{max}_{20}$	$(g^{-1}_{7/2}h^2_{11/2})^{max}_{27/2}$
$69/2^+$	10.251	9.94	-0.10	$(f^2_{7/2}h_{9/2}i_{13/2})^{max}_{17}$	$(d^{-2}_{5/2}h^3_{11/2})^{max}_{35/2}$
$69/2^-$	10.898	10.08	-0.15	$d^{-1}_{3/2}f^2_{7/2}h_{9/2}i^2_{13/2}$	$d^{-1}_{5/2}h^2_{11/2}$
$71/2^-$	10.692	10.33	-0.12	$f_{7/2}h_{9/2}i^2_{13/2}$	$d^{-2}_{5/2}h^3_{11/2}$
$(71/2^-)$	11.175	10.69	-0.15	$d^{-1}_{3/2}f^2_{7/2}h_{9/2}i^2_{13/2}$	$d^{-1}_{5/2}h^2_{11/2}$
$(73/2^+)$	11.326	10.79	-0.15	$d^{-1}_{3/2}f^2_{7/2}h_{9/2}i^2_{13/2}$	$(d^{-2}_{5/2})_0h^3_{11/2}$
$73/2^-$	11.493	11.00	-0.12	$f_{7/2}h_{9/2}i^2_{13/2}$	$d^{-2}_{5/2}h^3_{11/2}$
$75/2^-_1$	11.628	11.22	-0.11	$(f_{7/2}h_{9/2}i^2_{13/2})^{max}_{20}$	$(d^{-2}_{5/2}h^3_{11/2})^{max}_{35/2}$
$75/2^-_2$	11.857	11.65	-0.20	$(d^{-2}_{3/2})_0(f^3_{7/2}h_{9/2}i^2_{13/2})^{max}_{24}$	$(d^{-2}_{5/2})_0(h^3_{11/2})^{max}_{27/2}$
$75/2^-_3$	12.604	11.67	-0.11	$f_{7/2}h_{9/2}i^2_{13/2}$	$g^{-1}_{7/2}d^{-1}_{5/2}h^3_{11/2}$
$79/2^-_1$	12.620	12.80	-0.09	$(f_{7/2}h_{9/2}i^2_{13/2})^{max}_{20}$	$(g^{-1}_{7/2}d^{-1}_{5/2}h^3_{11/2})^{max}_{39/2}$
$(79/2^-_2)$	12.655	12.96	-0.21	$(d^{-2}_{3/2})_0f^3_{7/2}h_{9/2}i^2_{13/2}$	$d^{-2}_{5/2}h^3_{11/2}$
$79/2^-_3$	12.921	12.99	-0.18	$(d^{-2}_{3/2})_0(f^2_{7/2}h^2_{9/2}i^2_{13/2})^{max}_{26}$	$(d^{-2}_{5/2})_0(h^3_{11/2})^{max}_{27/2}$
$79/2^-_4$	13.751	13.25	-0.08	$(f_{7/2}h_{9/2}i^2_{13/2})^{max}_{20}$	$(g^{-2}_{7/2}h^3_{11/2})^{max}_{39/2}$
$83/2^-$	13.692	14.03	-0.21	$(d^{-2}_{3/2})_0(f^3_{7/2}h_{9/2}i^2_{13/2})^{max}_{24}$	$(d^{-2}_{5/2}h^3_{11/2})^{max}_{35/2}$
$(87/2^-)$	15.542	15.34	-0.20	$(d^{-2}_{3/2})_0(f^2_{7/2}h^2_{9/2}i^2_{13/2})^{max}_{26}$	$(d^{-2}_{5/2}h^3_{11/2})^{max}_{35/2}$
$(91/2^-)$	16.489	17.06	-0.19	$(d^{-2}_{3/2})_0(f_{7/2}h^2_{9/2}i^3_{13/2})^{max}_{28}$	$(d^{-2}_{5/2}h^3_{11/2})^{max}_{35/2}$

Table 3.

Relative population of the normal deformed states in ^{151}Tb fed by the yrast and first excited SD bands. The errors on the intensity values are less than 20 %. For each band the intensity of the strongest SD transition is assumed to be 100%.

SD-Yrast		SD-Excited 1	
Spin	Intensity(%)	Spin	Intensity (%)
$45/2^-$	4	$35/2^+$	24
$47/2^-$	15	$39/2^+$	27
$51/2_1{}^-$	5	$41/2^+$	9
$53/2^-$	4	$45/2^+$	40
$55/2^-$	10		
$(55/2^+)$	14		
$57/2^-$	7		
$63/2^-$	8		
$57/2^+$	7		
$61/2^+$	26		